

Assessment of Elasticity and Topography of *Aspergillus nidulans* Spores via Atomic Force Microscopy

Liming Zhao,¹ David Schaefer,² and Mark R. Marten^{1*}

Department of Chemical and Biochemical Engineering, University of Maryland, Baltimore County (UMBC), Baltimore,¹ and Department of Physics, Astronomy, and Geosciences, Towson University, Towson,² Maryland

Received 11 August 2004/Accepted 27 September 2004

Previous studies have described both surface morphology and adhesive properties of fungal spores, but little information is currently available on their mechanical properties. In this study, atomic force microscopy (AFM) was used to investigate both surface topography and micromechanical properties of *Aspergillus nidulans* spores. To assess the influence of proteins covering the spore surface, wild-type spores were compared with spores from isogenic *rodA*⁺ and *rodA*[−] strains. Tapping-mode AFM images of wild-type and *rodA*⁺ spores in air showed characteristic “rodlet” protein structures covering a granular spore surface. In comparison, *rodA*[−] spores were rodlet free but showed a granular surface structure similar to that of the wild-type and *rodA*⁺ spores. Rodlets were removed from *rodA*⁺ spores by sonication, uncovering the underlying granular layer. Both rodlet-covered and rodlet-free spores were subjected to nanoindentation measurements, conducted in air, which showed the stiffnesses to be 110 ± 10 , 120 ± 10 , and 300 ± 20 N/m and the elastic moduli to be 6.6 ± 0.4 , 7.0 ± 0.7 , and 22 ± 2 GPa for wild-type, *rodA*⁺ and *rodA*[−] spores, respectively. These results imply the rodlet layer is significantly softer than the underlying portion of the cell wall.

Fungal spores are of importance medically (25), agriculturally (9), and industrially (3) and provide fungi a natural means of reproduction, dispersion, and survival in adverse environmental conditions (22, 29). These benefits are in large part due to the spore cell wall, which has been compared to a man-made composite material (24). The wall is typically composed of various polysaccharide and protein components (17) and imparts great strength and resistance to chemical attack (24).

Knowledge of spore cell wall mechanical properties is necessary for a complete understanding of molecular component ultrastructure. Spore mechanical properties are also relevant during wall expansion which occurs as part of the germination process. It has been pointed out that changes in cell wall mechanical properties are central to the emergence of the germ tube (6, 21). While a number of studies have described surface morphology (4, 13, 14, 31) and adhesive properties (7, 27) of fungal spores, no information is currently available on their relevant micromechanical properties (e.g., elasticity).

The elasticity of an object can be described in terms of stress and strain. Stress is defined as the force applied per unit area, while strain is the resulting amount of deformation per unit length. The ratio of stress to strain (for an elastic material following Hooke's law) is defined as the elastic modulus (E), and describes the mechanical resistance of a material during elongation or compression. A large E implies a stiff or strong material, while a small E implies a softer material. To measure E , as well as other micromechanical properties, of different types of biological materials, a number of authors have used atomic force microscopy (AFM) (1, 2, 32, 33). To carry out these types of tests, a rigid AFM probe is used as an “indenter”

of the soft biological material, and the generated force-displacement data, or “force curves,” are then used to calculate the elastic modulus of the sample (28).

Previous electron microscopy studies have shown “rodlet” structures on the *Aspergillus nidulans* spore wall (18). These are composed primarily of protein (4, 10, 31) and are thought to serve several different functions (31). Rodlet structures are related to the wall structural gene *rodA* (26), in that *rodA*[−] spores lack the rodlet layer and are less hydrophobic than *rodA*⁺ spores (26). The goal in this work was to use AFM to study spores of *A. nidulans* by investigating surface morphology and calculating their elastic modulus. Three different *A. nidulans* strains (i.e., wild type, *rodA*⁺, and *rodA*[−]) were studied and compared. Surface morphology of spores was imaged by tapping-mode AFM, and force displacement measurements were used to determine the elastic modulus.

MATERIALS AND METHODS

Sample preparation. All *A. nidulans* strains used in this study were obtained from the Fungal Genetics Stock Center (Kansas City, Kans.): Glasgow wild type (A4), *rodA*[−] (A849; *pabaA1 yA2 ΔargB::trpCΔB ΔrodA::argB veA1 trpC801*), and *rodA*⁺ (A851; *pabaA1 yA2 ΔargB::trpCΔB veA1 trpC801*). Strains were stored as a frozen stock culture (5) and grown on potato dextrose agar (Difco, Detroit, Mich.) plates at 32°C for 3 to 4 days for sporulation. Round (12-mm diameter) glass coverslips (Fisher Scientific, Pittsburgh, Pa.) were cleaned with ethanol, coated with 0.01% poly-L-lysine (Sigma, St. Louis, Mo.) for 5 min, and used as the substrate for spore samples produced by the following two methods. “Untreated” spores were scratched from sporulated mycelial mats with an inoculating loop and, without further treatment, tapped over a poly-L-lysine-coated coverslip which was then used for AFM. Alternatively, “sonicated” spores were obtained from agar plates, suspended in sterile deionized water, and subjected to sonication (550 Sonic Dismembrator; Fisher Scientific, Pittsburgh, Pa.) at 4°C for 10 min with a 20% power output. After rinsing twice in deionized water, a drop of spore suspension was pipetted onto a poly-L-lysine-coated coverslip, allowed to dry in air (approximately 30 min), and subjected to AFM testing.

AFM imaging and force measurements. All experiments were performed in air, using a multimode atomic force microscope (Nanoscope IIIa; Digital Instruments, Santa Barbara, Calif.) equipped with a J-type piezoscanner. Both rotated TappingMode Etched Silicon Probes (RTESP; Digital Instruments) and Olym-

* Corresponding author. Mailing address: Department of Chemical and Biochemical Engineering, University of Maryland, Baltimore County (UMBC), 1000 Hilltop Circle, Baltimore, MD 21250. Phone: (410) 455-3439. Fax: (410) 455-1049. E-mail: marten@umbc.edu.

pus TappingMode Etched Silicon Probes (OTESP; Digital Instruments) were used for the imaging. Amplitude and height images were obtained in the tapping mode with a scan rate of 1 Hz and an integral gain of 0.3 to 0.5. The tapping force was adjusted by changing the set point voltage until high-resolution images were obtained in minimal tapping force. All images were recorded at room temperature and approximately 50% humidity. To perform force measurements, a spore was scanned in tapping mode to obtain a high-magnification image and to locate a position on the spore for force measurements. The cantilever tip was then withdrawn, and a force displacement curve was taken using the "trigger mode" (i.e., the piezo rises vertically until the preset maximal cantilever deflection, or maximal applied force, is reached and then retracts a distance equal to the preset vertical scan size). The cantilever deflection was calibrated by taking force curves on bare coverslips. To avoid large variation of spring constants of individual cantilevers, only one RTESP cantilever and one OTESP were used in all force measurements. The spring constants of these cantilevers were determined to be 61 and 82 N/m, respectively, by measuring the resonance frequencies of the cantilevers (11). The silicon tip was found to have a radius of 10 nm by scanning several calibration gratings and extracting the tip shape from the resulting image (data not shown). Force curve data were used to calculate stiffness and E as described in the next section. Statistical comparison was performed by using single-factor analysis of variance, and the results are presented with the P value.

Theory. The presented micromechanical calculations assume that, in response to the external, concentrated, normal force exerted by the AFM tip, the *A. nidulans* spore wall is indented instead of bent or stretched. This assumption is based on the fact that *A. nidulans* spores possess cell walls several hundred nanometers in thickness (6), while the deformation depth involved in this study is only 5 to ~10 nm.

Pharr et al. (23) showed that for any axis-symmetric indenters with smooth profiles, the unloading stiffness, $dF/d\delta$, is related to the projected contact area, A , and the reduced elastic modulus, E_r , in the following equation:

$$\frac{dF}{d\delta} = 2E_r \left(\frac{A}{\pi} \right)^{1/2} \quad (1)$$

Here F is the applied force and δ is the indentation depth.

In the contact region of the force curves, the displacement of the sample will produce a deflection of the cantilever. If both the cantilever and the sample are infinitely hard, then the cantilever deflection, d , will equal the sample displacement, z (assuming the initial contact point as the origin). Otherwise, the sample displacement equals the sum of the cantilever deflection and the indentation on the specimen:

$$z = d + \delta \quad (2)$$

The applied force, F , can be determined by assuming Hooke's law behavior (valid for small displacements):

$$F = k \times d \quad (3)$$

where k is the cantilever spring constant, determined by measuring resonant frequency and using known geometric and material properties of the cantilever (11):

$$k = 2\pi^2 l^3 w v_o^3 \sqrt{\rho^3/E_i} \quad (4)$$

where l , w , ρ , E_i , and v_o are the length, width, density, E , and resonance frequency of the cantilever, respectively.

At small indentation depths, as in this work, the apex of the AFM tip can be assumed to have a spherical profile with a radius of curvature, R . This assumption was tested by imaging the AFM probes used here over sharp calibration spikes. It was found that the contour of the lower portion of the tip could be approximated well by a hemisphere (data not shown). The projected area of elastic contact is then given by the geometry (Fig. 1A)

$$A = \pi(2R\delta_p - \delta_p^2) \quad (5)$$

where δ_p is the indentation depth below the circle of contact which is found from reference 15

$$\delta_p = \frac{\delta_i + \delta_r}{2} \quad (6)$$

and the maximal indentation depth, δ_i and residual depth, δ_r , are determined experimentally (Fig. 1B).

The initial portion of the unloading curve represents an elastic contact, and the

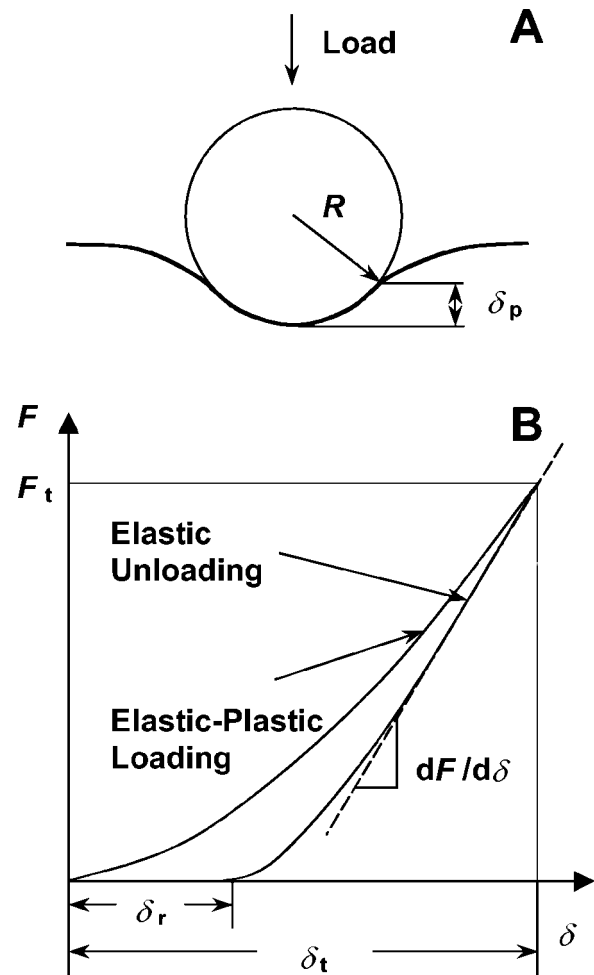


FIG. 1. Schematic illustration of (A) elastic-plastic contact between a rigid spherical indenter and a specimen and (B) concurrent load versus displacement curve used to determine stiffness and the elastic modulus. R is the indenter radius, F_t is the maximum applied force, δ_p is the indentation depth below the circle of contact, δ_i is the maximum indentation depth, δ_r is the residual depth, and $dF/d\delta$ is the unloading stiffness.

slope $dF/d\delta$ is defined as the stiffness, S (Fig. 1B), and calculated from the observed slope, m , of the experimental force curves (d versus z) according to

$$S = \frac{dF}{d\delta} = k \frac{m}{1-m} \quad (7)$$

In equation 1, E_r is used to correct the effects of nonrigid indenters on penetration measurement. Thus, the elastic modulus of the material can be calculated according to the following relation (23):

$$\frac{1}{E_r} = \frac{1-\nu^2}{E} + \frac{1-\nu_i^2}{E_i} \quad (8)$$

where E and E_i are the elastic moduli and ν and ν_i are the Poisson ratios of the specimen and the indenter, respectively. Typically, soft biological tissues are treated as incompressible materials (Poisson ratio = 0.5) because of their high water content. However, in this study, testing was conducted in air and thus water content of spores was likely to be relatively low (21). When this is the case, one can generally expect values of the Poisson ratio in the interval from 0 to 0.5 for most practical materials (8). We note that in this range variations for corresponding E values determined from equation 8 are less than 15% of the modulus for the maximum ν (= 0.5); therefore, an average value $\nu = 0.3$ was assumed for the spores. For a silicon indenter, E_i and ν_i are 130 GPa and 0.28, respectively (<http://www.ioffe.rssi.ru>).

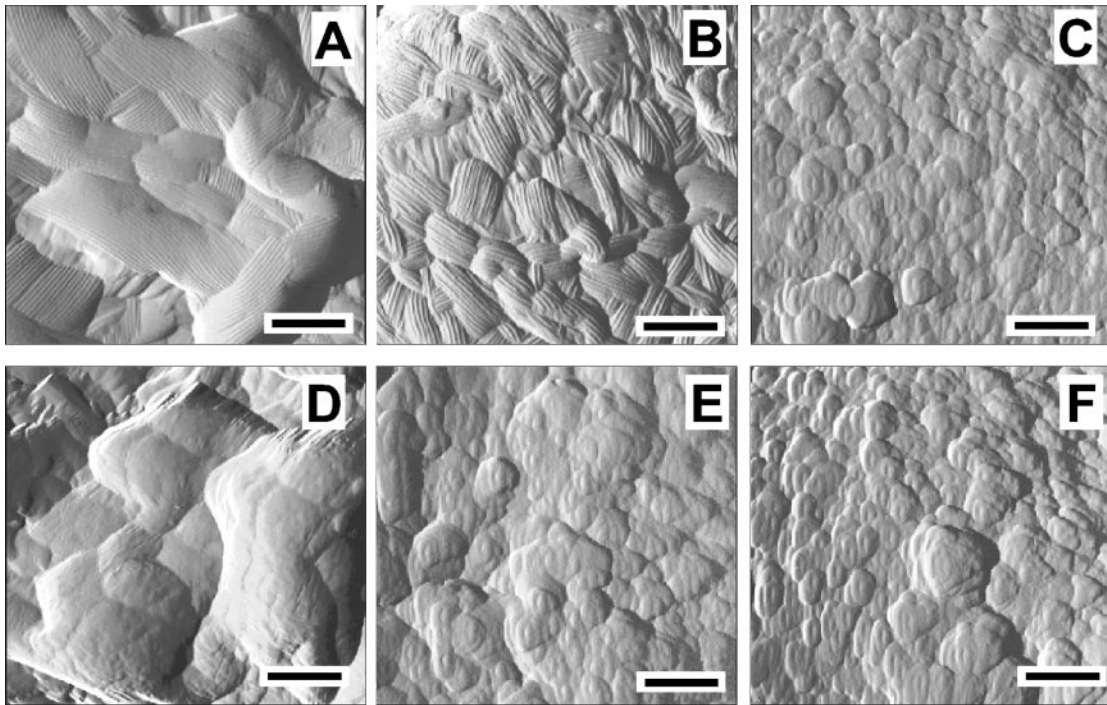


FIG. 2. Images generated by AFM in the tapping mode of the surface morphology of (A to C) untreated and (D to F) sonicated spores. (A and D) wild type; (B and E) *rodA*⁺; and (C and F) *rodA*⁻. Bar length, 0.2 μ m.

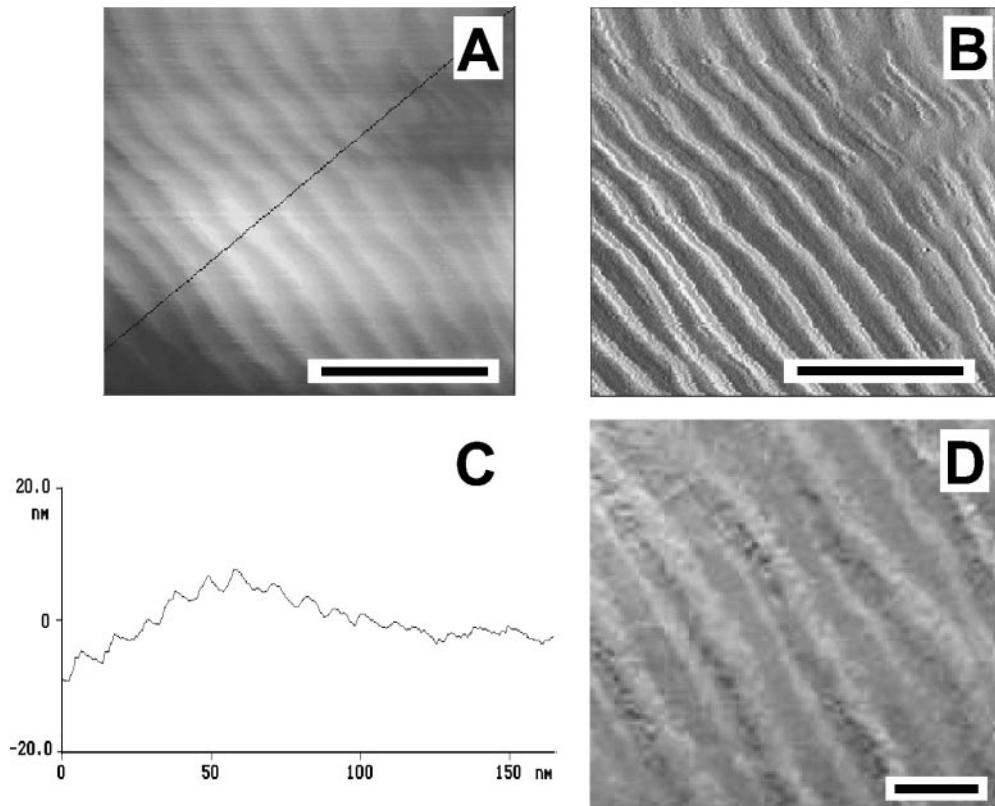


FIG. 3. Images (A; height) and (B; amplitude) show the rodlet structure on the wild-type spores. (C) Cross-section along the line in panel A reveals the periodicity of the rodlets. Image D shows rodlets are apparently composed of two strands. Bar lengths: 50 nm in panels A and B and 10 nm in panel D.

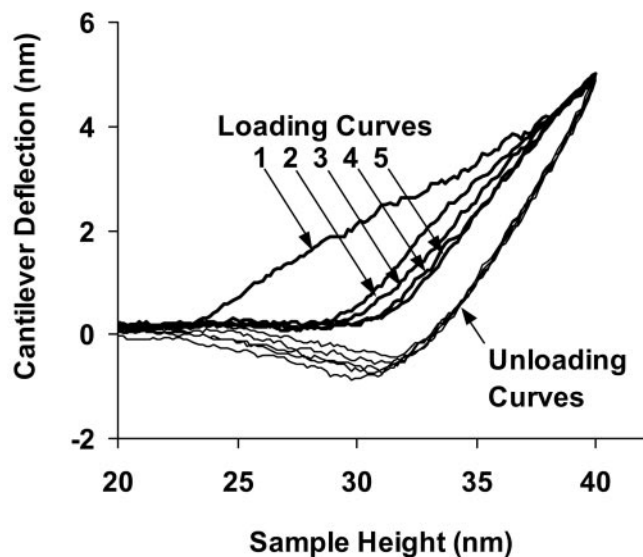


FIG. 4. Typical force curves for five sequential tests at the same position on the same untreated wild-type spore, measured with an RTESP ($k = 61$ N/m). Loading curves (thick lines) are labeled 1 through 5. Unloading curves (thin lines) overlap.

RESULTS AND DISCUSSION

Spore surface morphology. Tapping-mode AFM was used to assess fungal spore surface morphology (Fig. 2). Untreated wild-type spores (Fig. 2A) had a rough surface, consisting of granular domains (approximately $0.4 \mu\text{m}$ in length) with a rodlet layer on each. By comparison, $rodA^+$ spores (Fig. 2B) showed similar rodlet structures on smaller domains (approximately $0.2 \mu\text{m}$ in length), while $rodA^-$ spores (Fig. 2C) exhibited granular materials on a rodlet-free surface. Previous studies have shown that rodlet structures are directly related to the rodlet-encoding gene *rodA* and that deletion of *rodA* leads to loss of the rodlet layer (26). Our AFM images are consistent with these findings. Additionally, the observation that $rodA^+$ spores exhibit smaller rodlet domains than wild-type spores indicates that the $rodA^+$ strain may harbor a mutation affecting rodlet domain organization.

To determine the affinity of the rodlet layer for the spore

surface, *A. nidulans* spores were subjected to AFM imaging after sonication (Fig. 2D to F). Both wild-type and $rodA^+$ strains were observed to lose nearly all rodlets, uncovering the underlying region of granular materials. In comparison, no perceivable morphological changes were observed on $rodA^-$ spores before and after the sonication (Fig. 2C and F). Furthermore, we found the surface features of the sonicated $rodA^+$ spores were quite similar to those of $rodA^-$ spores. These observations imply the rodlet layer does not adhere strongly to spore surface and can be removed by hydrodynamic shear.

Higher-resolution images revealed additional rodlet detail (Fig. 3). On both wild-type and $rodA^+$ strains, the rodlet layer covered the entire surface of each domain, with each rodlet being approximately 10 nm in diameter and hundreds of nanometers in length. These observations are consistent with previous studies employing electron microscopy (14, 16) or contact mode AFM (13). Our images, however, reveal additional detail, as each rodlet appears to be composed of two strands, each of which is approximately 3 nm in diameter (Fig. 3D). Previous studies have shown rodlets are composed primarily of the protein hydrophobin (20, 30, 31), whose diameter is speculated to be approximately 3.1 nm (12), in close agreement with the strand diameters found here.

Apparent elastic moduli of fungal spores. With the cantilever tip used as a microindenter, force-displacement measurements (i.e., force curves) were made and used to calculate the elastic modulus of the spores. As the normal spore wall apparently has at least two layers (rodlet and underlying granular material), with their true elastic moduli unknown, an apparent elastic modulus, \hat{E} , was defined to represent responses from both layers in force displacement measurements.

To assess reproducibility, force curves were repeatedly taken at the same position on a number of wild-type spores (Fig. 4). For the first several cycles, the approaching curves are not reproducible, implying plastic deformation or viscoelasticity that is not reversible on the time scale of the measurement. After enough cycles, force curves are reproducible, but instead of overlapping, the loading and unloading force curves exhibit hysteresis, implying viscous contributions from the spore. Because the initial portion of the unloading curves represents an

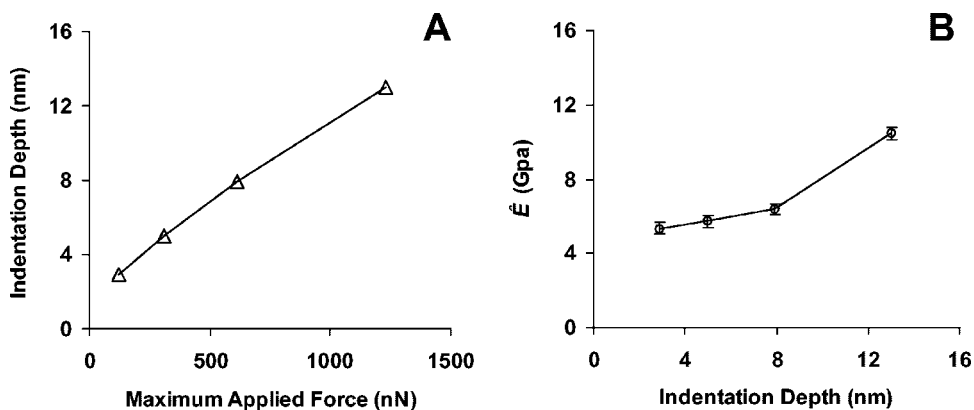


FIG. 5. Effect of increasing maximum applied force on (A) indentation depth and (B) apparent elastic modulus, \hat{E} , for a wild-type spore, measured with an RTESP ($k = 61$ N/m). Error bars represent the standard error of the measurements shown in Fig. 7.

elastic contact, data from unloading curves were used for calculation of \hat{E} .

To determine the effect of the maximum force applied by the AFM cantilever (i.e., trigger threshold deflection), a series of force curves were collected at the same position on a wild-type spore, increasing the maximum applied force in each subsequent test. Small indentations (normally several nanometers) were applied. As shown in Fig. 5A, the depth of cantilever indentation increased with the maximal force applied (a visible permanent impression was made on the spore surface at 2,400 nN; data not shown). \hat{E} calculated from these tests also increased correspondingly (Fig. 5B), implying that the underlying layer was more rigid than the rodlet layer as the tip sensed more and more contributions from the underlying layer. Thus, to ensure consistent measurements of \hat{E} , force curves were generated with a maximum applied force of 650 nN (unless specified).

Typical force curves taken both on bare glass (calibration) and of different spore samples are shown in Fig. 6. One notable difference between the four force curves is that they have different slopes in the contact region. Glass is assumed to be infinitely hard and has a steep linear contact region (slope = 1; Fig. 6A). In the spore force curves (Fig. 6B to D) the lower slope implies a softer surface. Force curves were taken on a number of different spore samples (5 to 11 spores for each category, 3 to 5 force curves for each spore at different positions); values of stiffness (S) were determined to be 110 ± 10 , 120 ± 10 , and 300 ± 20 N/m; and apparent elastic moduli (\hat{E}) were determined to be 6.6 ± 0.4 , 7.0 ± 0.7 , and 22 ± 2 GPa for untreated wild-type, $rodA^+$, and $rodA^-$ spores, respectively (Fig. 7). The two $rodA$ -bearing strains (e.g., wild type and $rodA^+$) had similar S ($P = 0.15$) and \hat{E} ($P = 0.57$) values. In contrast the $rodA^-$ strains had larger S and \hat{E} values than the $rodA^+$ strain ($P < 0.001$). This implies the rodlet-covered surfaces are softer than the rodlet-free surface. However, this difference was eliminated after the removal of the rodlet layer. When both $rodA$ -bearing strains were sonicated, they exhibited similar granular, rodlet-free surfaces and had similar S ($P = 0.62$) and \hat{E} ($P = 0.11$) values (Fig. 7). Typically, sonicated spores had larger S and \hat{E} values than untreated spores, partially due to the loss of the rodlet layer. In addition, it is noted that $rodA^-$ spores also showed slightly larger S and \hat{E} values after the sonication (without a perceivable morphological variation; see Fig. 2C and 4C), which implies the sonication or other unknown factors affect the determinations of mechanical properties.

It has been shown that fungal cell walls are sensitive to KOH, laminarinase, pronase, and chitinase treatment (19). According to these results, it was suggested that wall components such as amorphous α -1,3 glucan, β -1,3 glucan, and glycoproteins make up the wall matrix, while cross-linked polysaccharides such as chitin are primarily maintained in the inner wall layers (19). Our data imply that the rodlet-covered surface is softer than the rodlet-free surface. Thus, the rodlet protein surface layer is apparently softer than the complex matrix of cross-linked polysaccharides in the underlying wall structure. This matrix imparts great strength and has been compared to a man-made composite material (24). The relatively high wall elastic modulus we determined implies it is difficult for dormant spores to germinate, in which the yielding of the cell wall

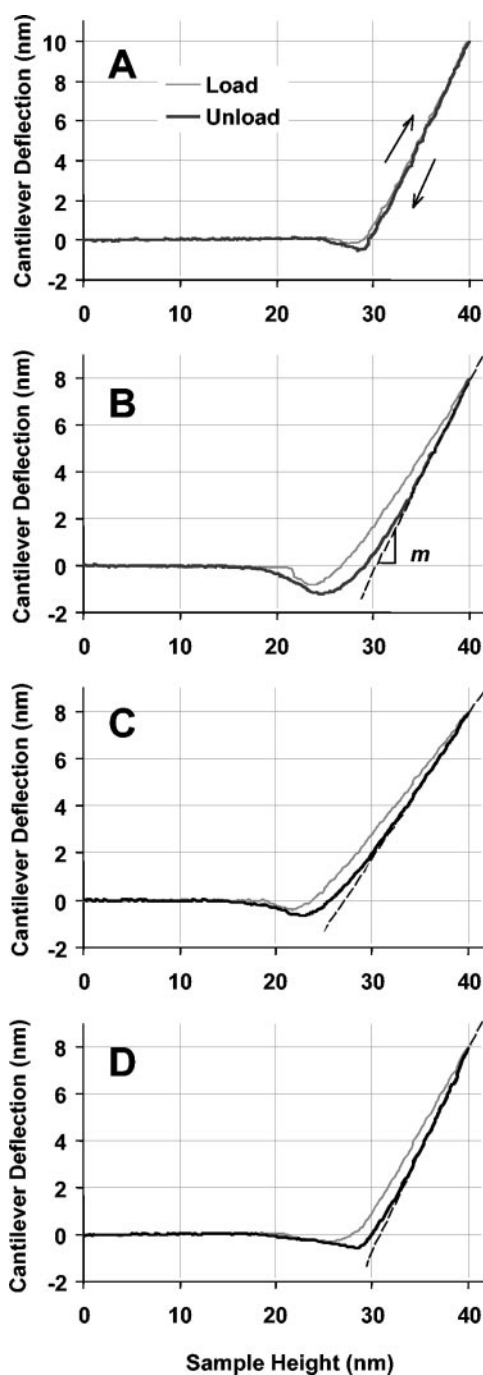


FIG. 6. Force-displacement curves measured on the surface of (A) bare glass, (B) $rodA^-$, (C) $rodA^+$, and (D) “sonicated” $rodA^+$ with an OTESP silicon probe, $k = 82$ N/m. Dashed lines in the contact region represent initial slopes (m) of the unloading curves, which were determined to be 0.79, 0.60, and 0.84, respectively, for $rodA^-$, $rodA^+$, and “sonicated” $rodA^+$ spores.

to the increasing turgor inside the cell leads to cell germination and the protrusion of germ tubes. Therefore, a decrease in wall strength or wall softening is assumed to accompany spore germination (21).

Conclusion. While a number of studies are available on spore surface morphology, little is known about spore microme-

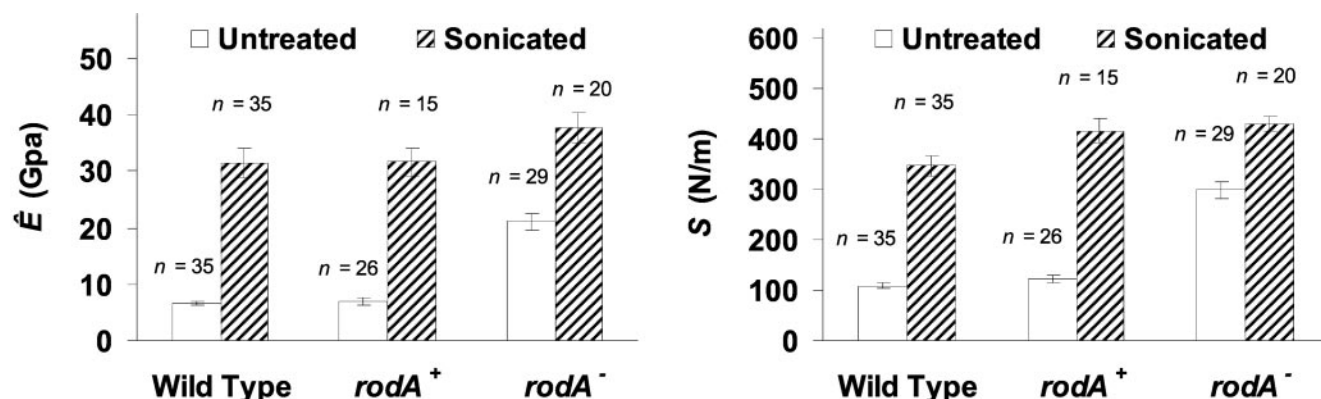


FIG. 7. Average values of (A) the apparent elastic modulus, \hat{E} , and (B) the stiffness, S , for the wild-type, *rodA*⁺, and *rodA*⁻ *A. nidulans* spores, measured with an RTESP ($k = 61$ N/m on the wild type) and an OTESP ($k = 82$ N/m on *rodA*⁺ and *rodA*⁻ spores). Error bars represent the standard error of the measurements.

chanical properties. In this study, AFM was used to visualize the surface of fungal spores and to make measurements of the spore wall stiffness and elastic modulus. In agreement with others, we find the spore surface to be covered with a rodlet layer, apparently composed of protein. This layer was easily removed by sonication. Tests of spores with and without this rodlet layer show the stiffness and elastic modulus of *rodA*⁺ spores are approximately one-third the values of *rodA*⁻ spores. This implies that the rodlet layer is significantly softer than the underlying portion of the cell wall.

ACKNOWLEDGMENTS

This work was supported by grants BES-9876012 and BES-9906586 from the National Science Foundation and by Novozymes North America, Inc.

We thank M. P. Nandakumar for his assistance in fungal culture.

REFERENCES

- A-Hassan, E., W. F. Heinz, M. D. Antonik, N. P. D'Costa, S. Nageswaran, C.-A. Schoenberger, and J. H. Hoh. 1998. Relative microelastic mapping of living cells by atomic force microscopy. *Biophys. J.* **74**:1564–1578.
- Arnoldi, M., M. Fritz, E. Bauerlein, M. Radmacher, E. Sackmann, and A. Boulbitch. 2000. Bacterial turgor pressure can be measured by atomic force microscopy. *Physiol. Rev. E* **62**:1034–1044.
- Arora, D. K., R. P. Elander, and K. G. Mukerji (ed.). 1992. Handbook of applied mycology, vol. 4, p. 3–4. Marcel Dekker, New York, N.Y.
- Beever, R. E., and G. P. Dempsey. 1978. Function of rodlets on the surface of fungal spores. *Nature* **272**:608–610.
- Bhargava, S., M. P. Nandakumar, A. Roy, K. S. Wenger, and M. R. Marten. 2003. Pulsed feeding during fed-batch fungal fermentation leads to reduced viscosity without detrimentally affecting protein expression. *Biotechnol. Bioeng.* **81**:341–347.
- Border, D. J., and A. P. J. Trinci. 1970. Fine structure of the germination of *Aspergillus nidulans* conidia. *Trans. Br. Mycol. Soc.* **54**:143–146.
- Bowen, W. R., R. W. Lovitt, and C. J. Wright. 2000. Direct quantification of *Aspergillus niger* spore adhesion in liquid using an atomic force microscope. *J. Colloid Interface Sci.* **228**:428–433.
- Brandrup, J., and E. H. Immergut (ed.). 1989. Polymer handbook. Wiley, New York, N.Y.
- Charudattan, R. 1991. The mycoherbicide approach with plant pathogens, p. 24–57. In D. O. TeBeest (ed.), *Microbial control of weeds*. Chapman and Hall, London, United Kingdom.
- Claverie-Martin, F., M. R. Diaz-Torres, and M. J. Geoghegan. 1986. Chemical composition and electron microscopy of the rodlet layer of *Aspergillus nidulans* conidia. *Curr. Microbiol.* **14**:221–225.
- Cleveland, J. P., S. Manne, D. Bocek, and P. K. Hansma. 1993. A nondestructive method for determining the spring constant of cantilevers for scanning force microscopy. *Rev. Sci. Instrum.* **64**:403–405.
- de Vocht, M. L., K. Scholtmeijer, E. W. van der Vegte, O. M. de Vries, N. Sonveaux, H. A. Wosten, J. M. Ruyschaert, G. Hadziloannou, J. G. Wessels, and G. T. Robillard. 1998. Structural characterization of the hydrophobin SC3, as a monomer and after self-assembly at hydrophobic/hydrophilic interfaces. *Biophys. J.* **74**:2059–2068.
- Dufréne, Y. F., C. J. P. Boonaert, P. A. Gerin, M. Asther, and P. G. Rouxhet. 1999. Direct probing of the surface ultrastructure and molecular interactions of dormant and germinating spores of *Phanerochaete chrysosporium*. *J. Bacteriol.* **181**:5350–5354.
- Dute, R. R., J. D. Weete, and A. E. Rushing. 1989. Ultrastructure of dormant and germinating conidia of *Aspergillus ochraceus*. *Mycologia* **81**:772–782.
- Field, J. S., and M. V. Swain. 1993. A simple predictive model for spherical indentation. *J. Mater. Res.* **8**:297–306.
- Gerin, P. A., M. Asther, U. B. Sleytr, and P. G. Rouxhet. 1994. Detection of rodlets in the outer wall region of conidiospores of *Phanerochaete chrysosporium*. *Can. J. Microbiol.* **40**:412–416.
- Gooday, G. W. 1994. Cell walls, p. 43–60. In N. A. R. Gow and G. M. Gadd (ed.), *The growing fungus*. Chapman & Hall, London, United Kingdom.
- Hess, W. M., and D. L. Stocks. 1969. Surface characteristics of *Aspergillus* conidia. *Mycologia* **61**:560–571.
- Hunsley, D., and J. H. Burnett. 1970. The ultrastructure architecture of the walls of some hyphal fungi. *J. Gen. Microbiol.* **62**:203–218.
- Lugones, L. G., J. S. Bosscher, K. Scholtmeijer, O. M. de Vries, and J. G. Wessels. 1996. An abundant hydrophobin (ABH1) forms hydrophobic rodlet layers in *Agaricus bisporus* fruiting bodies. *Microbiology* **142**:1321–1329.
- Money, N. P. 1994. Osmotic adjustment and the role of turgor in mycelial fungi, p. 67–88. In K. Esser and P. A. Lemke (ed.), *The mycota*, vol. 1. Springer-Verlag, Berlin, Germany.
- Oshero, N., and G. S. May. 2001. The molecular mechanisms of conidial germination. *FEMS Microbiol. Lett.* **199**:153–160.
- Pharr, G. M., W. C. Oliver, and F. R. Brotzen. 1992. On the generality of the relationship among contact stiffness, contact area, and the elastic modulus during indentation. *J. Mater. Res.* **7**:613–617.
- Ruiz-Herrera, J. 1992. Fungal cell wall: structure, synthesis, and assembly. CRC Press, Boca Raton, Fla.
- Sternberg, S. 1994. The emerging fungal threat. *Science* **266**:1632–1634.
- Stringer, M. A., R. A. Dean, T. C. Sewall, and W. E. Timberlake. 1991. Rodletless, a new *Aspergillus* developmental mutant induced by directed gene inactivation. *Genes Dev.* **5**:1161–1171.
- van der Aa, B. C., R. M. Michel, M. Asther, M. T. Zamora, P. G. Rouxhet, and Y. F. Dufréne. 2001. Stretching cell surface macromolecules by atomic force microscopy. *Langmuir* **17**:3116–3119.
- Vinckier, A., and G. Semenza. 1998. Measuring elasticity of biological materials by atomic force microscopy. *FEBS Lett.* **430**:12–16.
- Wessels, J. G. 1993. Fruiting in the higher fungi. *Adv. Microb. Physiol.* **34**:147–202.
- Wessels, J. G. 1997. Hydrophobin, proteins that change the nature of the fungal surface. *Adv. Microb. Physiol.* **38**:1–45.
- Wosten, H. A., and M. L. de Vocht. 2000. Hydrophobins, the fungal coat unravelled. *Biochim. Biophys. Acta* **1469**:79–86.
- Yao, X., M. Jericho, D. Pink, and T. Beveridge. 1999. Thickness and elasticity of gram-negative murein sacculi measured by atomic force microscopy. *J. Bacteriol.* **181**:6865–6875.
- Yao, X., J. Walter, S. Burke, S. Stewart, M. H. Jericho, D. Pink, R. Hunter, and T. J. Beveridge. 2002. Atomic force microscopy and theoretical considerations of surface properties and turgor pressures of bacteria. *Colloids Surf. B* **23**:213–230.